Cell Reports, Volume *30*

Supplemental Information

Tissue-Resident PDGFRα^+ Progenitor Cells Contribute to Fibrosis versus Healing in a Context- and Spatiotemporally Dependent Manner

Maria Paola Santini, Daniela Malide, Gabriel Hoffman, Gaurav Pandey, Valentina D'Escamard, Aya Nomura-Kitabayashi, Ilsa Rovira, Hiroshi Kataoka, Jordi Ochando, Richard P. Harvey, Toren Finkel, and Jason C. Kovacic

Figure S1

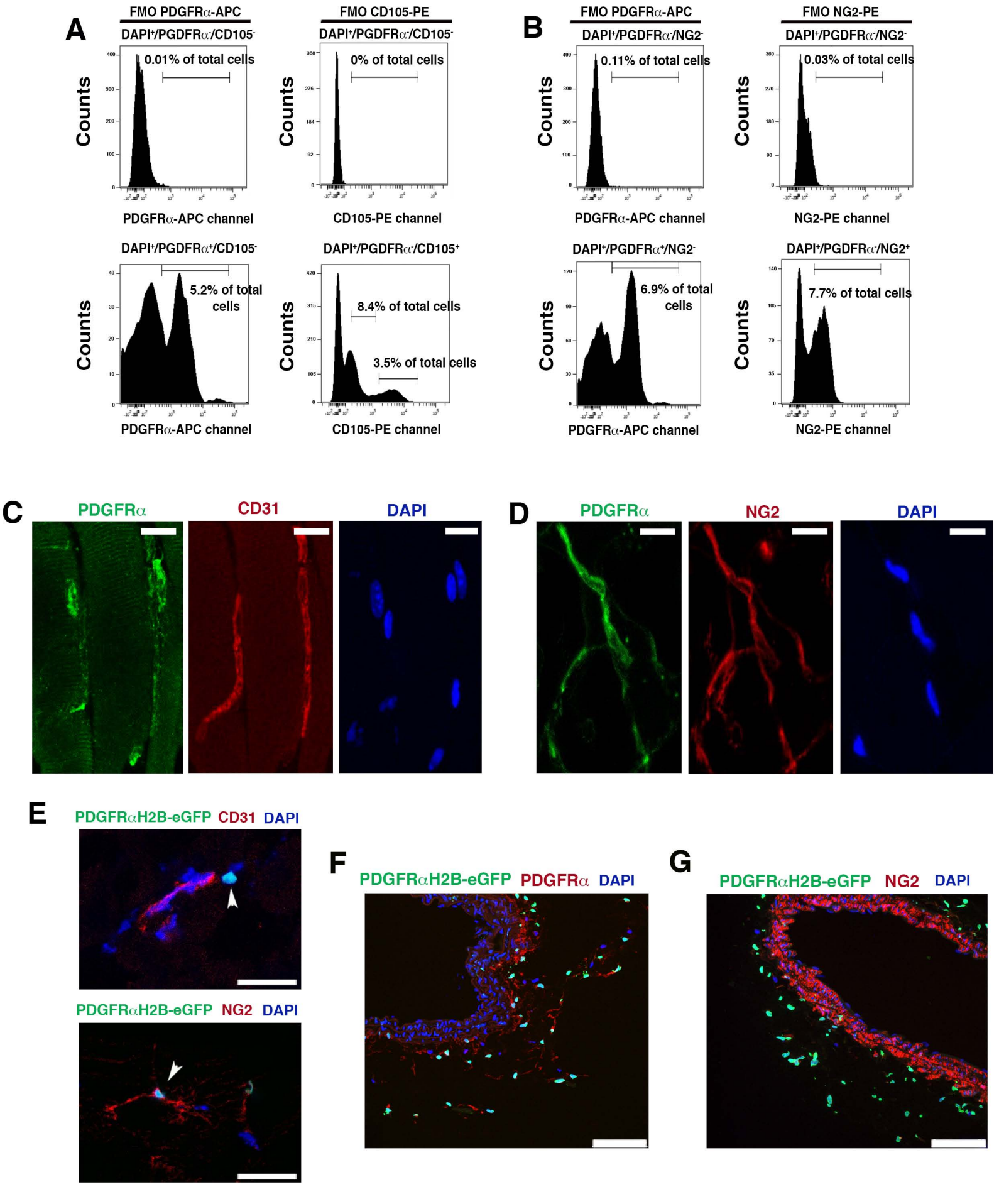
A
FMO PDGFRα-APC
DAPI+/PGDFRα-/CD105-
0.01% of total cells
Counts
PDGFRα-APC channel
FMO CD105-PE
DAPI+/PGDFRα-/CD105-
0% of total cells
Counts
CD105-PE channel
DAPI+/PGDFRα+/CD105-
5.2% of total cells
Counts
PDGFRα-APC channel
DAPI+/PGDFRα-/CD105+
8.4% of total cells
3.5% of total cells
Counts
CD105-PE channel
B
FMO PDGFRα-APC
DAPI+/PGDFRα-/NG2-
0.11% of total cells
Counts
PDGFRα-APC channel
FMO NG2-PE
DAPI+/PGDFRα-/NG2-
0.03% of total cells
Counts
NG2-PE channel
DAPI+/PGDFRα+/NG2-
6.9% of total cells
Counts
PDGFRα-APC channel
DAPI+/PGDFRα-/NG2+
7.7% of total cells
Counts
NG2-PE channel
C
PDGFRα
CD31
DAPI
D
PDGFRα
NG2
DAPI
E
PDGFRαH2B-eGFP CD31 DAPI
PDGFRαH2B-eGFP NG2 DAPI
F
PDGFRαH2B-eGFP PDGFRα DAPI
G
PDGFRαH2B-eGFP NG2 DAPI

Figure S1. Flow cytometric and histological assessment of PDGFRα$^+$ cells. Related to Figure 1.
(A-B) Fluorescence minus one (FMO) controls were used to set the gates of all flow cytometric analyses shown in Figure 1A-B. Representative FMO controls are shown for PDGFRα$^+$ cells co-positive for CD105 **(S1A)** and NG2 **(S1B)**. These were selected because they demonstrate FMO controls for a population with both a high and low co-positive population (S1A; CD105) and single co-positive population (S1B; NG2). All analyses were performed in n=3 independent experiments. **(C-D)** Single color channels of immunofluorescence for PDGFRα$^+$ cells with CD31 (S1C; corresponds to Figure 1C) or NG2 (S1D; corresponds to Figure 1E) in skeletal muscle of 4 month old healthy uninjured mice, performed as described in Star Methods. Images represent merged z-stacks acquired with a Leica SP5 DM confocal. Scale bars 20µm. **(E)** Immunofluorescence analysis of skeletal muscle from 4 month old *PdgfrαH2B-eGfp* mice. White arrowheads show GFP$^+$NG2$^+$ co-positive cells (lower panels) or proximity of GFP$^+$ cells with CD31$^+$ cells (upper panel). Staining was performed with rat monoclonal CD31 and mouse monoclonal NG2 antibody. Images represent merged z-stacks acquired with a Leica SP5 DM confocal. Scale bars 25µm. **(F-G)** Thoracic aortas from 4 month old *PdgfrαH2B-eGfp* mice were isolated and analyzed for expression of PDGFRα **(F)** and NG2 **(G)**. Fresh frozen 10µm sections were stained with anti-GFP 1:500 Abcam, ab13970; PDGFRα, 1:50, Cell signaling, 3174P and NG2, 1:50 Abcam, ab83178. Images represent z-stacks acquired with a Leica SP5 DM confocal. Scale bars 75µm.

Figure S2

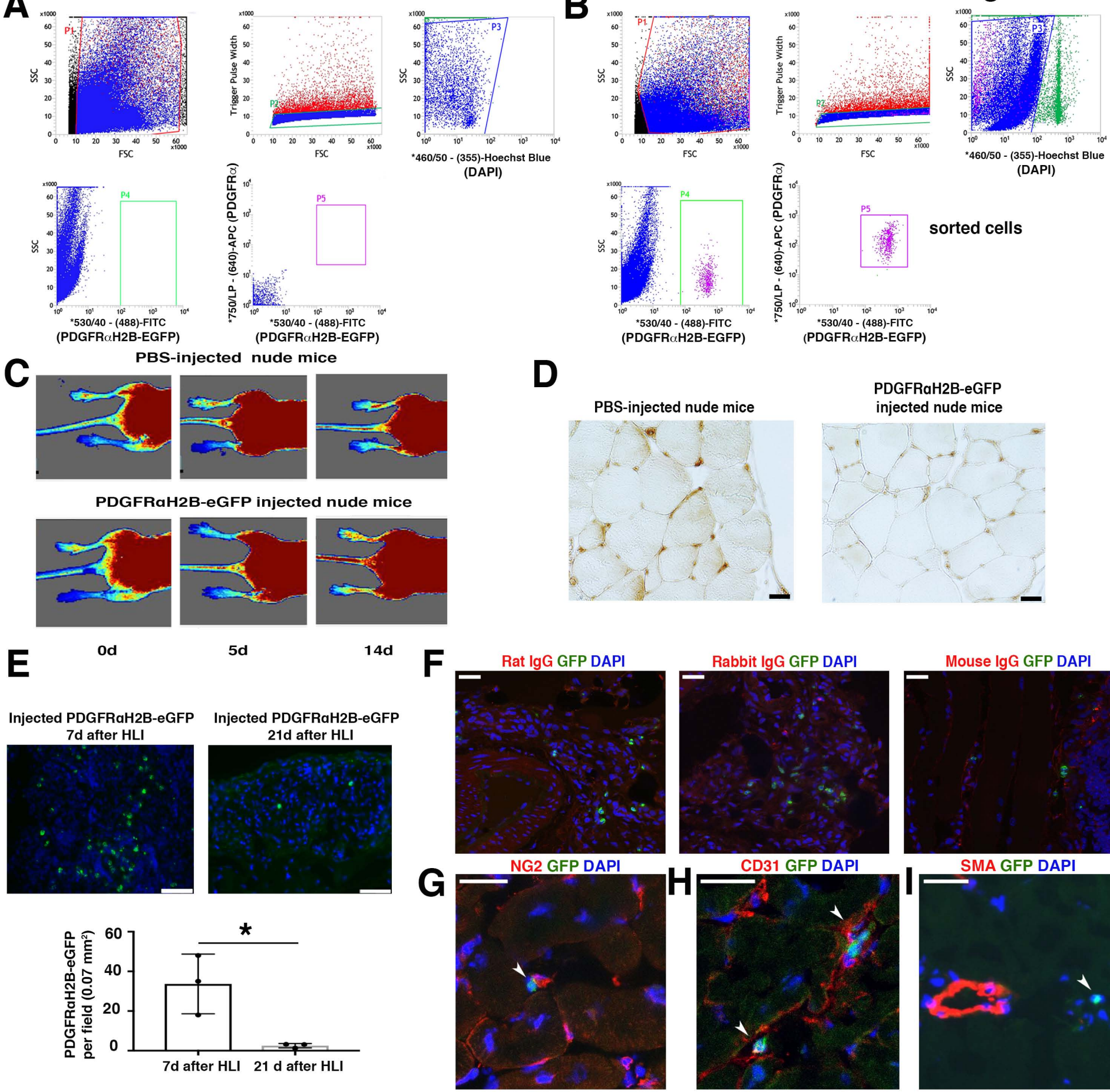
A
B
SSC
FSC
Trigger Pulse Width
*460/50 - (355)-Hoechst Blue
(DAPI)
*530/40 - (488)-FITC
(PDGFRαH2B-EGFP)
*750/LP - (640)-APC (PDGFRα)
sorted cells
C
PBS-injected nude mice
PDGFRαH2B-eGFP injected nude mice
0d
5d
14d
D
PBS-injected nude mice
PDGFRαH2B-eGFP
injected nude mice
E
Injected PDGFRαH2B-eGFP
7d after HLI
Injected PDGFRαH2B-eGFP
21d after HLI
PDGFRαH2B-eGFP
per field (0.07 mm²)
7d after HLI
21 d after HLI
F
Rat IgG GFP DAPI
Rabbit IgG GFP DAPI
Mouse IgG GFP DAPI
G
NG2 GFP DAPI
H
CD31 GFP DAPI
I
SMA GFP DAPI

Figure S2. PDGFRα$^+$ cell function in tissue revascularization after hindlimb ischemia. Related to Figures 2 and 3.

Undifferentiated GFP$^+$PDGFRα$^+$ co-positive cells from 3 month old *PdgfrαH2B-eGfp* male mice were injected into the adductor muscle of 7 month old nude female mice 24 hours after HLI. **(A-B)** Adductor skeletal muscles were isolated from 3 month old male WT control mice and left un-labeled (also without DAPI) to set FACS gates for sorting **(A)**, or labeled with anti-PDGFRα APC-conjugated antibody and DAPI to sort for GFP$^+$PDGFRα$^+$ co-positive cells from *PdgfrαH2B-eGfp* mice **(B)**. The Hoechst Blue channel distinguishes DAPI$^-$ live cells (gate P3) from dead (DAPI$^+$) cells. Taking the live DAPI$^-$ population, FITC was used to specify for *PdgfrαH2B-eGfp*$^+$ cells (gate P4). In the final panel, the FITC (x axis) and APC (y axis) specifies for cells double positive for GFP and APC (after labeling with anti-PDGFRα APC-conjugated antibody) (gate P5). Sorted live GFP$^+$PDGFRα$^+$ co-positive cells were processed for further analyses (RNAseq and adoptive transfer experiments). **(C)** Representative images of blood flow acquired with a MoorFLPI Full Field Laser Perfusion Imager Review V4.0 (Moor Instruments Ltd) after HLI. **(D)** Representative capillary images 21 days after HLI induction using isolectin B4 staining on 8µm paraffin sections. Sections were stained with biotinylated isolectin B4 (Sigma Aldrich, Inc) overnight at 4°C. Capillaries were counted from 4 separate sections for each mouse (n=3 per group) in an area of 0.1mm^2. Scale bar 20µm. **(E)** Approximately 7x10^5 GFP$^+$PDGFRα$^+$ co-positive cells were injected in the adductor muscle after HLI and these tissue samples were analyzed at 7 and 21 days for their GFP$^+$ cell content. Scale bars 50µm. Images were acquired with a Leica DMi8, Application Suite X, DCF365FX camera. Pictures are representative of n=3 mice. Quantification was performed using Image J. GFP$^+$PDGFRα$^+$ co-positive cells were counted in each field where the presence of the cells was maximal as described in Star Methods. Data represent mean ± SD. *P<0.05. **(F)** Control staining corresponding to Figure 3. Seven days after HLI induction and adoptive transfer of undifferentiated GFP$^+$PDGFRα$^+$ co-positive cells, injected cells were tracked by nuclear GFP expression and co-staining with rat (control IgG for CD31), mouse (control IgG for αSMA) and rabbit IgG (control IgG for NG2) as described in Star Methods to analyze antibody specificity. Scale bar 25µm. Z-stacks images were acquired with a Leica SP5 DM confocal microscope. **(G-I)** Three weeks after HLI induction and adoptive transfer of undifferentiated GFP$^+$PDGFRα$^+$ cells, injected cells were tracked by nuclear GFP expression (white arrowheads) and co-staining with rabbit anti-mouse NG2 **(G)**, rat anti-mouse CD31 antibody to detect capillaries **(H)** and Cy3-conjugated anti-αSMA antibody to detect large vessels **(I)**. Scale bars 20µm. Images are representative of n=3 independent experiments. Z-stack images in (G-H) were obtained with a Leica SP5 DM confocal microscope. Image in (I) was obtained with a Leica CTR 5500 microscope and DFC340FX camera.

Figure S3

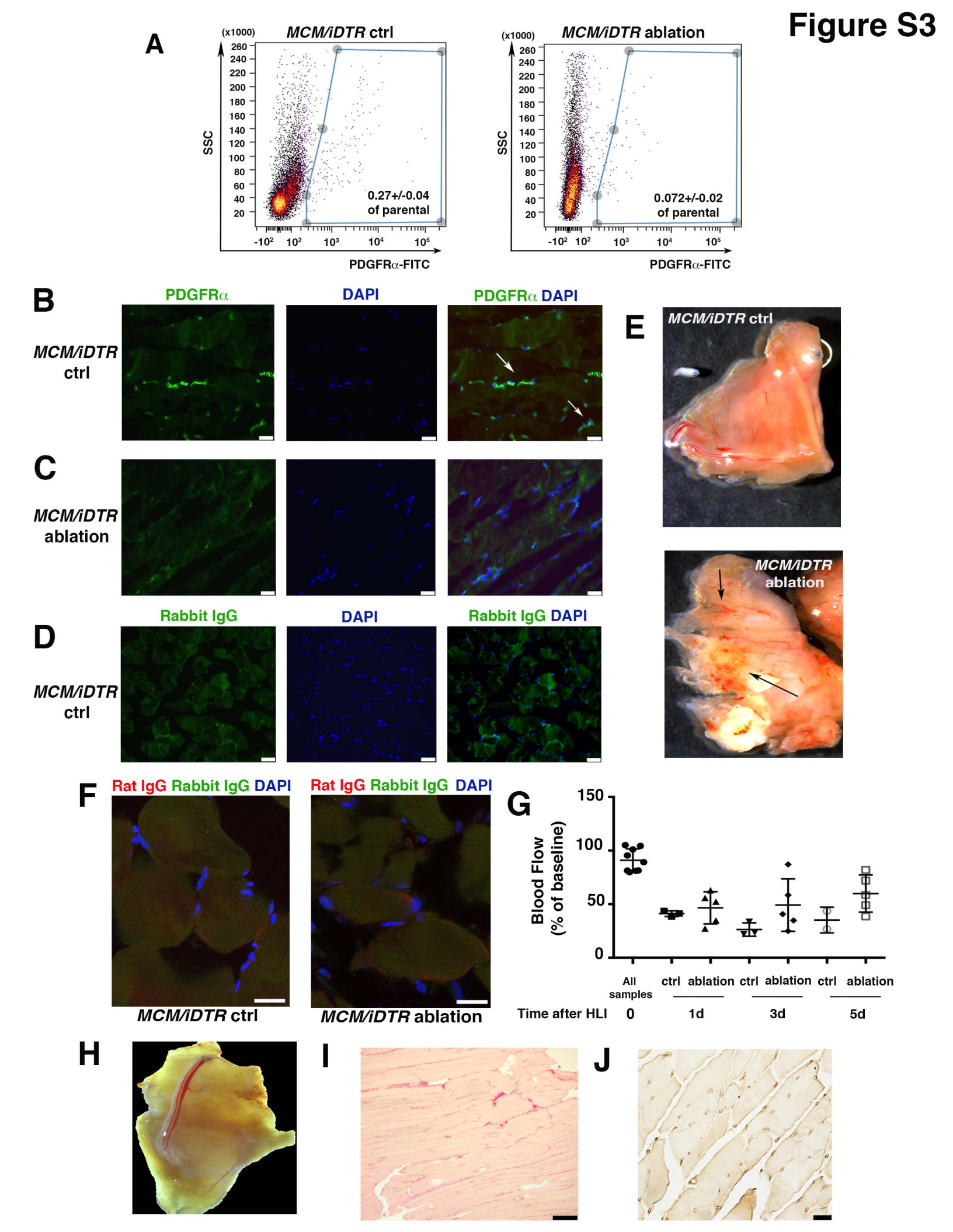
A
MCM/iDTR ctrl
(x1000)
SSC
PDGFRα-FITC
0.27+/-0.04
of parental
MCM/iDTR ablation
0.072+/-0.02
of parental
B
PDGFRα
DAPI
PDGFRα DAPI
MCM/iDTR
ctrl
C
MCM/iDTR
ablation
D
Rabbit IgG
DAPI
Rabbit IgG DAPI
MCM/iDTR
ctrl
E
MCM/iDTR ctrl
MCM/iDTR
ablation
F
Rat IgG Rabbit IgG DAPI
MCM/iDTR ctrl
MCM/iDTR ablation
G
Blood Flow
(% of baseline)
All
samples
ctrl
ablation
Time after HLI
0
1d
3d
5d
H
I
J

Figure S3. Modulation of tissue revascularization after PDGFRα$^+$ cell ablation. Related to Figure 4. **(A)** Flow cytometric analysis of hindlimbs from *MCM$^+$/iDTR$^{+/-}$* mice treated with tamoxifen and DTX (*MCM/iDTR* ablation) versus peanut oil and DTX (*MCM/iDTR* control, ctrl) 5 days after HLI induction. PDGFRα$^+$ cells were labeled with FITC-conjugated anti-PDGFRα antibody (1μg per million cells) (eBioscience). Data were analyzed using the Cytobank web application. Each *MCM/iDTR* ablation mouse was validated with flow cytometric analysis and only those showing successful ablation of PDGFRα$^+$ cells were used for further experiments. Ablation was successful in 4 out of 5 treated animals, and the panels here represent the flow cytometric data in n=4 animals for *MCM/iDTR* ablation and n=4 for *MCM/iDTR* controls in a fraction of the skeletal muscles. **(B-D)** Cell ablation was also verified by immunofluorescence staining with anti-PDGFRα antibody on 8μm frozen sections of a small hindlimb tissue fragment from *MCM/iDTR* controls (n=3) and *MCM/iDTR* ablated mice (n=3) after HLI. Arrows in (B) show interstitial PDGFRα$^+$ cells in control mice, while in (C) no PDGFRα$^+$ cells are seen in *MCM/iDTR* mice after cell ablation. Control rabbit IgG antibody (D) was used on *MCM/iDTR* control mice. Areas shown are adjacent those with ischemic injury. Scale bars 25μm. Images in B-D were acquired with a Leica DMi8, Application Suite X, and a DFC365FX camera. **(E)** Adductor muscles from *MCM/iDTR* ctrl and ablated mice were harvested 5 days after HLI induction and images were obtained under a dissection microscope. Arrows show macroscopically visible hemorrhage. **(F)** Immunofluorescence analysis of *MCM/iDTR* ablated and ctrl adductor muscles with rat IgG (red) and rabbit IgG (green) that correspond to Figures 4D-E. Scale bars 20μm. Images are representative of n=3 independent experiments. Images were obtained with a confocal Leica SP5 DM as z-stacks. **(G)** Blood flow was assessed as indicated in Star Methods. Eight mice were analyzed at time 0 and after HLI were divided randomly as control (peanut oil and DTX treated mice *MCM/iDTR*, n=3) or ablation (tamoxifen and DTX treated mice *MCM/iDTR* ablated, n=5) mice. Data represent mean ± SD and are analyzed by one-way ANOVA followed by Tukey's multiple comparison test. There were no differences between the control and ablated groups at any time point. **(H-J)** Representative panels showing **(H)** whole muscles, **(I)** Picrosirius Red (scale bar 200μm) and **(J)** isolectin B4 staining (scale bar 25μm) of *MCM/iDTR* ablated adductor muscles in sham-operated (no HLI) mice. Image in (H) was obtained under a dissection microscope. Images in (I and J) were obtained with a Leica DMi8, Application Suite X, and a DCM2900 camera.

Figure S4

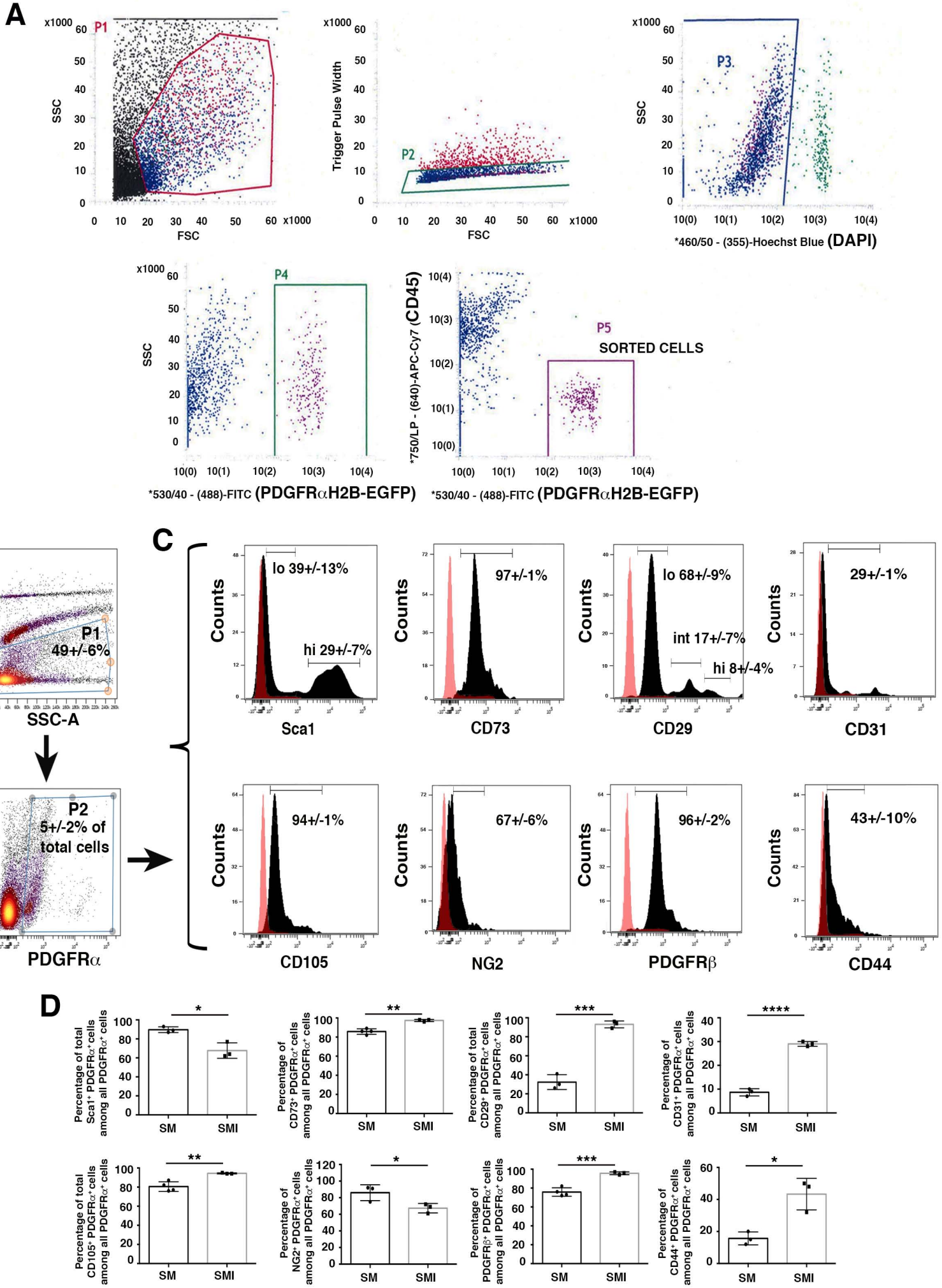
A
P1
SSC
FSC
x1000
P2
Trigger Pulse Width
P3
*460/50 - (355)-Hoechst Blue (DAPI)
P4
*530/40 - (488)-FITC (PDGFRαH2B-EGFP)
P5
SORTED CELLS
*750/LP - (640)-APC-Cy7 (CD45)
B
DAPI
P1
49+/-6%
SSC-A
P2
5+/-2% of total cells
PDGFRα
C
Counts
lo 39+/-13%
hi 29+/-7%
Sca1
97+/-1%
CD73
lo 68+/-9%
int 17+/-7%
hi 8+/-4%
CD29
29+/-1%
CD31
94+/-1%
CD105
67+/-6%
NG2
96+/-2%
PDGFRβ
43+/-10%
CD44
D
Percentage of total Sca1+ PDGFRα+ cells among all PDGFRα+ cells
Percentage of CD73+ PDGFRα+ cells among all PDGFRα+ cells
Percentage of total CD29+ PDGFRα+ cells among all PDGFRα+ cells
Percentage of CD31+ PDGFRα+ cells among all PDGFRα+ cells
Percentage of total CD105+ PDGFRα+ cells among all PDGFRα+ cells
Percentage of NG2+ PDGFRα+ cells among all PDGFRα+ cells
Percentage of PDGFRβ+ PDGFRα+ cells among all PDGFRα+ cells
Percentage of CD44+ PDGFRα+ cells among all PDGFRα+ cells
SM
SMI

Figure S4. Characterization of PDGFRα$^+$ cells at early time points after hindlimb ischemia. Related to Figure 5.

(A) FACS was performed on digested skeletal muscle from *PdgfrαH2B-eGfp* mice 7 days after HLI induction. Cells were labeled with 1μg/ml of DAPI to distinguish live (DAPI$^-$) from dead (DAPI$^+$) cells (gate P3, upper right panel) and with anti-CD45-APC-Cy7 (1μg/million cells). From the live GFP$^+$ cell population (P4, lower left panel) we identified GFP$^+$PDGFRα$^+$ cells (P5, lower right panel), which were almost entirely CD45$^-$ (P5) (only rare, isolated CD45$^+$GFP$^+$PDGFRα$^+$ cells were detected – too few to permit reliable quantitation). GFP$^+$PDGFRα$^+$ cells were sorted and underwent RNAseq. FACS plots are representative of 4 independent experiments. **(B and C)** As separate experiments to (A) and using WT mice at 10-12 weeks of age, flow cytometric analysis of skeletal muscle PDGFRα$^+$ cells was performed using Cytobank software for phenotypic characterization. Cells were extracted 7 days after HLI from skeletal muscle with Liberase DL (Roche) and labeled for 30 minutes at room temperature with anti-PDGFRα-APC antibody and **(C)** PE-conjugated antibodies for endothelial (CD31), mesenchymal (Sca1, CD73, CD105, CD29, CD44) and pericyte markers (NG2 and PDGFRβ). Cells were gated as a live DAPI$^-$ population (B, gate P1) and further as PDGFRα-APC$^+$ (B, gate P2). In C, the panels represent the co-expression expression of PDGFRα$^+$ cells for these markers. Flow cytometric plots are representative of n=3 independent experiments for all markers. As controls, cells extracted from skeletal muscle were labeled with APC- and PE-conjugated IgG isotype antibodies for the indicated markers and as described in Star Methods. Cells were gated first as a live DAPI$^-$ population and representative histograms are overlaid (pink peaks) with the indicated mesenchymal, endothelial and pericyte markers. FMO controls were also performed for this experiment and are shown in Figures S5A-B. **(D)** Quantification by flow cytometry of PDGFRα$^+$ cells co-positive for endothelial (CD31), mesenchymal (Sca1, CD73, CD105, CD29, CD44) and perivascular markers (NG2 and PDGFRβ) in physiologic conditions (uninjured; SM) *vs* 7 days after HLI (SMI). Percentage of total population for Sca1$^+$PDGFRα$^+$ and CD105$^+$PDGFRα$^+$ co-positive cells includes the low and high populations, whereas for CD29$^+$PDGFRα$^+$ includes the low, high and intermediate populations. Data represent mean ± SD. Asterisks indicate *P<0.05, **P<0.01, ***P<0.001 and ****P<0.0001. For Sca1, NG2, CD44 and CD31 SM is n=3, whereas for CD105, CD29, CD73 and PDGFRβ SM is n=4. SMI samples are n=3.

Figure S5

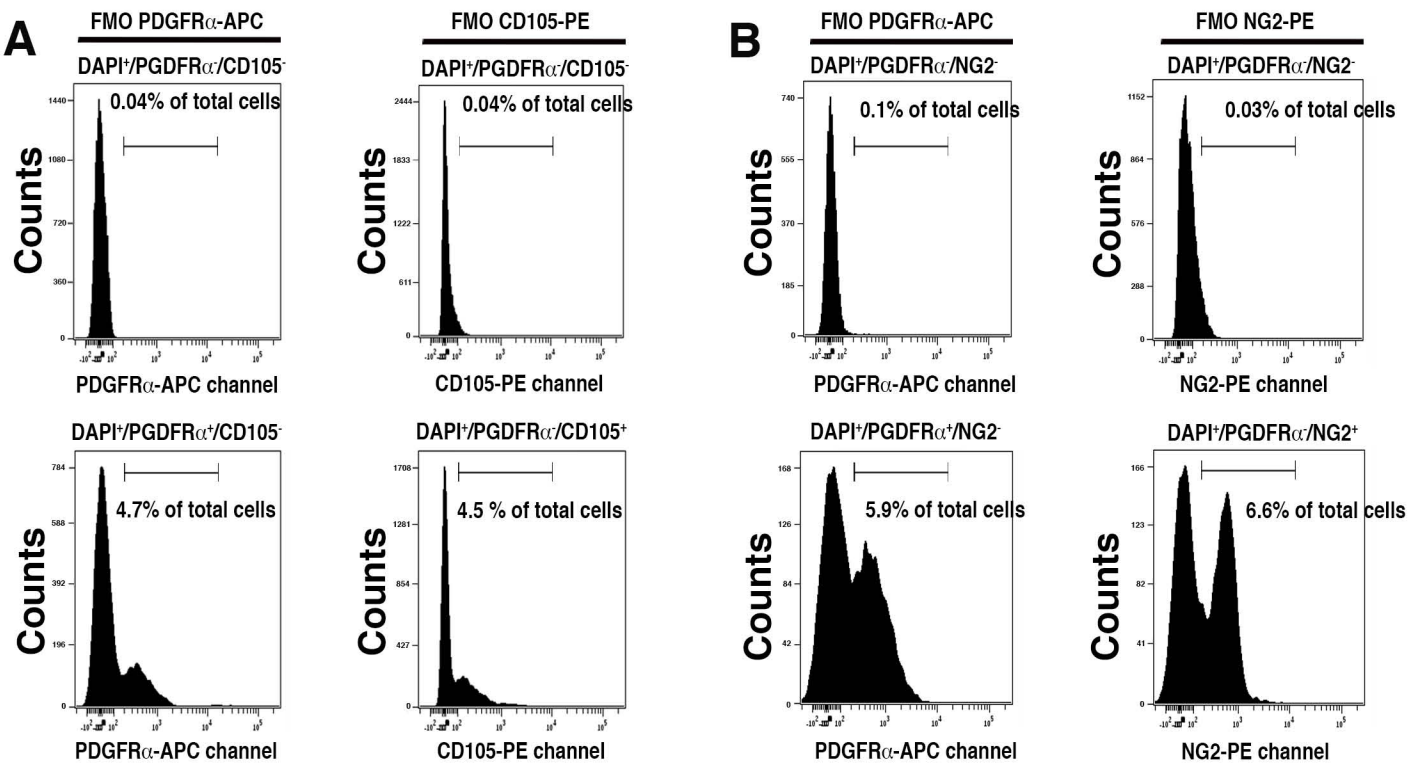
A
FMO PDGFRα-APC
DAPI+/PGDFRα-/CD105-
0.04% of total cells
Counts
PDGFRα-APC channel
FMO CD105-PE
DAPI+/PGDFRα-/CD105-
0.04% of total cells
Counts
CD105-PE channel
B
FMO PDGFRα-APC
DAPI+/PGDFRα-/NG2-
0.1% of total cells
Counts
PDGFRα-APC channel
FMO NG2-PE
DAPI+/PGDFRα-/NG2-
0.03% of total cells
Counts
NG2-PE channel
DAPI+/PGDFRα+/CD105-
4.7% of total cells
Counts
PDGFRα-APC channel
DAPI+/PGDFRα-/CD105+
4.5 % of total cells
Counts
CD105-PE channel
DAPI+/PGDFRα+/NG2-
5.9% of total cells
Counts
PDGFRα-APC channel
DAPI+/PGDFRα-/NG2+
6.6% of total cells
Counts
NG2-PE channel

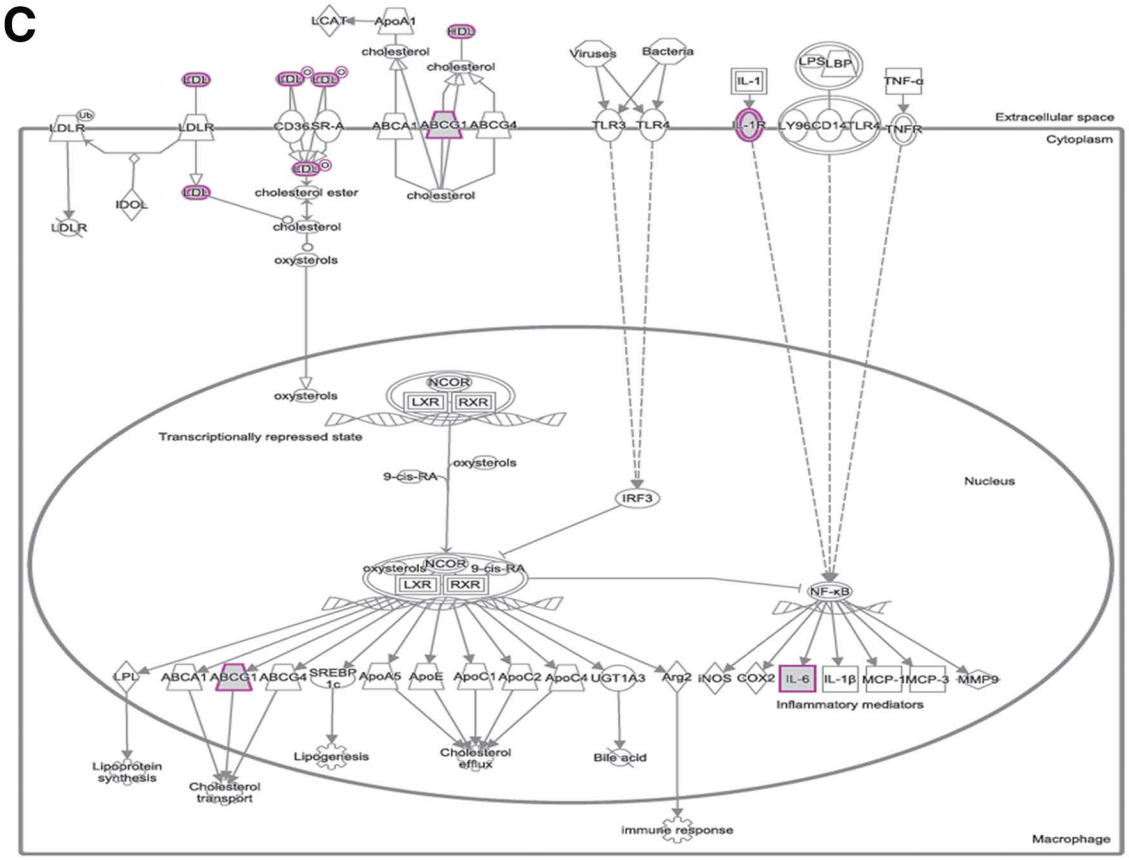
C
LCAT
ApoA1
HDL
cholesterol
LDL
LDLR
CD36SR-A
ABCA1 ABCG1 ABCG4
Viruses
Bacteria
TLR3 TLR4
IL-1
IL-1R
LPS LBP
LY96 CD14 TLR4
TNF-α
TNFR
Extracellular space
Cytoplasm
IDOL
cholesterol ester
oxysterols
NCOR
LXR
RXR
Transcriptionally repressed state
9-cis-RA
IRF3
Nucleus
NF-κB
LPL
ABCA1 ABCG1 ABCG4
SREBP 1c
ApoA5 ApoE ApoC1 ApoC2 ApoC4
UGT1A3
Arg2
iNOS COX2
IL-6 IL-1β MCP-1 MCP-3 MMP9
Inflammatory mediators
Lipoprotein synthesis
Cholesterol transport
Lipogenesis
Cholesterol efflux
Bile acid
Immune response
Macrophage

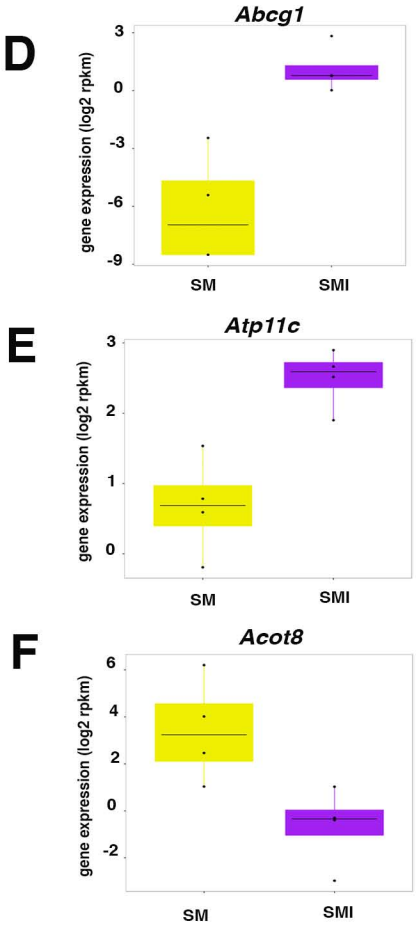
D
Abcg1
gene expression (log2 rpkm)
SM
SMI
E
Atp11c
gene expression (log2 rpkm)
SM
SMI
F
Acot8
gene expression (log2 rpkm)
SM
SMI

Figure S5. Characterization of PDGFRα$^+$ cells at early time points after hindlimb ischemia. Related to Figure 4.

(A-B) Fluorescence minus one (FMO) controls were used to set the gates of the analyses shown in Figures S4B-C. Representative FMO controls are shown for PDGFRα$^+$ cells co-positive for CD105 **(A)** and NG2 **(B)**. As per Figure S1 these were again selected because they demonstrate FMO controls for a population with both a high and low co-positive population (S5A; CD105) and single co-positive population (S5B; NG2). All the analyses were performed in n=3 independent experiments. **(C)** IPA networks based on differential gene expression of GFP$^+$PDGFRα$^+$ cells 7 days after HLI, as compared to these cells from uninjured *PdgfrαH2B-eGfp* mice, show modulation of LXR/RXR signaling (which is implicated in lipid transport). Genes/proteins are illustrated as nodes and molecular relationships as connecting lines between two nodes (direct relationships as normal lines; indirect relationships as dashed lines). Molecular relationships are supported by at least one literature reference, or by canonical information stored in the Ingenuity Pathway Knowledge Base. Purples nodes represent genes of interest (differentially expressed in GFP$^+$PDGFRα$^+$ cells from SM versus SMI hindlimbs), while white nodes represent hubs that were added by the IPA algorithm to connect a set of genes of interest. **(D-F)** RNAseq data showing gene expression differences in GFP$^+$PDGFRα$^+$ cells of transcripts related to lipid transport in SM versus SMI samples, including upregulation of *Abcg1* and *Atp11c* (cholesterol transporter) and downregulation of *Acot8* (hydrolysis of AcylCoA).

Figure S6

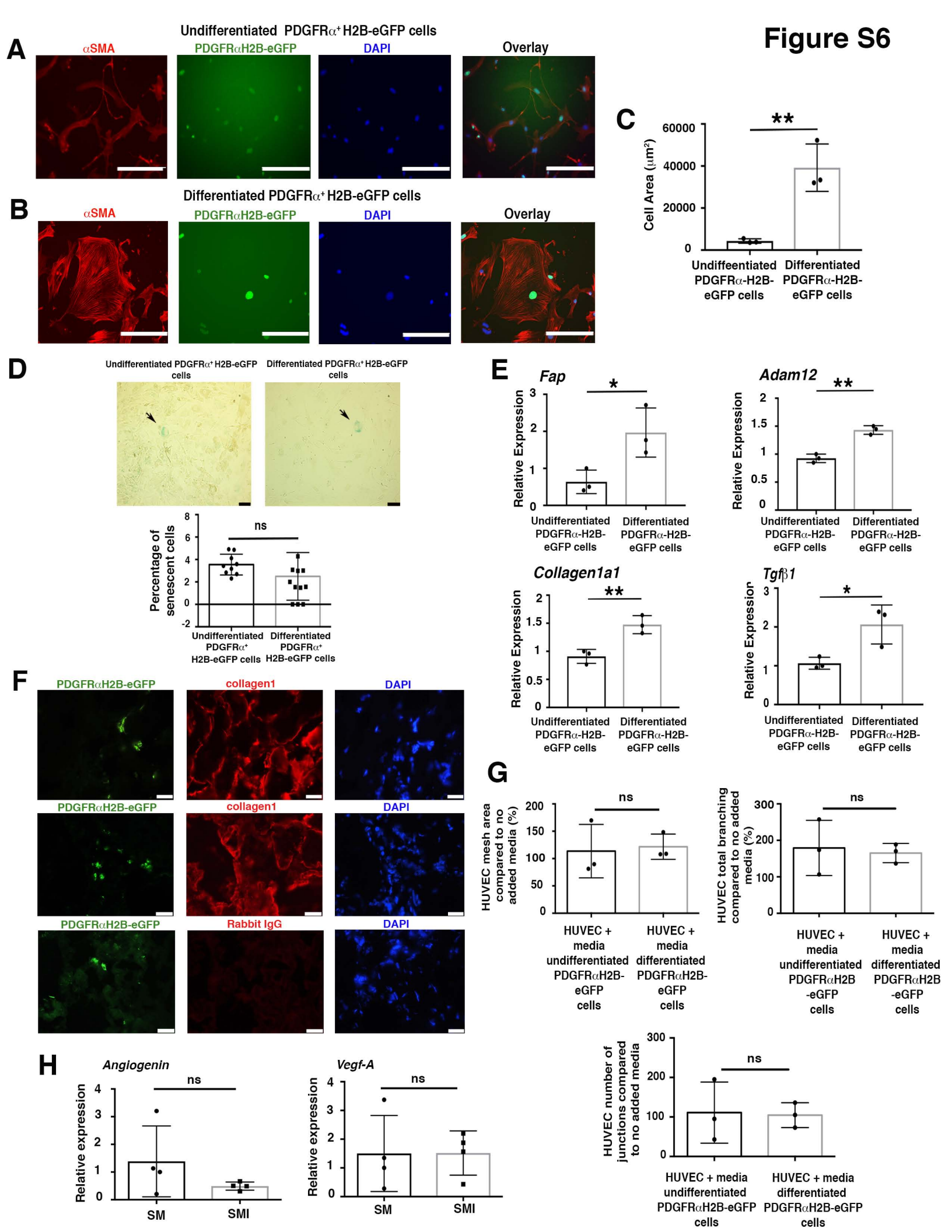
A
Undifferentiated PDGFRα+ H2B-eGFP cells
αSMA
PDGFRαH2B-eGFP
DAPI
Overlay
B
Differentiated PDGFRα+ H2B-eGFP cells
αSMA
PDGFRαH2B-eGFP
DAPI
Overlay
C
Cell Area (μm²)
60000
40000
20000
0
**
Undifferentiated PDGFRα-H2B-eGFP cells
Differentiated PDGFRα-H2B-eGFP cells
D
Undifferentiated PDGFRα+ H2B-eGFP cells
Differentiated PDGFRα+ H2B-eGFP cells
Percentage of senescent cells
8
6
4
2
0
-2
ns
Undifferentiated PDGFRα+ H2B-eGFP cells
Differentiated PDGFRα+ H2B-eGFP cells
E
Fap
Relative Expression
3
2
1
0
*
Undifferentiated PDGFRα-H2B-eGFP cells
Differentiated PDGFRα-H2B-eGFP cells
Adam12
Relative Expression
2
1.5
1
0.5
0
**
Undifferentiated PDGFRα-H2B-eGFP cells
Differentiated PDGFRα-H2B-eGFP cells
Collagen1a1
Relative Expression
2
1.5
1
0.5
0
**
Undifferentiated PDGFRα-H2B-eGFP cells
Differentiated PDGFRα-H2B-eGFP cells
Tgfβ1
Relative Expression
3
2
1
0
*
Undifferentiated PDGFRα-H2B-eGFP cells
Differentiated PDGFRα-H2B-eGFP cells
F
PDGFRαH2B-eGFP
collagen1
DAPI
PDGFRαH2B-eGFP
collagen1
DAPI
PDGFRαH2B-eGFP
Rabbit IgG
DAPI
G
HUVEC mesh area compared to no added media (%)
200
150
100
50
0
ns
HUVEC + media undifferentiated PDGFRαH2B-eGFP cells
HUVEC + media differentiated PDGFRαH2B-eGFP cells
HUVEC total branching compared to no added media (%)
300
200
100
0
ns
HUVEC + media undifferentiated PDGFRαH2B-eGFP cells
HUVEC + media differentiated PDGFRαH2B-eGFP cells
H
Angiogenin
Relative expression
4
3
2
1
0
ns
SM
SMI
Vegf-A
Relative expression
4
3
2
1
0
ns
SM
SMI
HUVEC number of junctions compared to no added media
300
200
100
0
ns
HUVEC + media undifferentiated PDGFRαH2B-eGFP cells
HUVEC + media differentiated PDGFRαH2B-eGFP cells

Figure S6. Function of undifferentiated versus differentiated PDGFRα$^+$ cells. Related to Figure 6. **(A-D)** GFP$^+$PDGFRα$^+$ co-positive cells were FACS-sorted from *PdgfrαH2B-eGfp* mice and plated in DMEM supplemented with 10% FBS and grown in either 5% O_2 without passaging (undifferentiated PDGFRα$^+$ cells) or 20% O_2 and passaged once (differentiated PDGFRα$^+$ cells). Cells were stained with Cy3-conjugated anti-αSMA antibody at 1:500 dilution for 1 hour at room temperature. Compared to undifferentiated cells **(A)**, differentiated PDGFRα$^+$ cells exhibited a fine cytoskeletal structure composed of αSMA fibers **(B)**. Images were acquired with an EVOS AMG cell imaging system (Thermo Fisher Scientific). **(C)** Differentiated PDGFRα$^+$ cells had a hypertrophied phenotype with increased cell area as measured by ImageJ software. Data are the average of n=3 independent experiments in each cell group. Student's t-test was performed using GraphPad Prism version 6.00. Data represent mean ± SD. **P<0.01. **(D)** β-galactosidase activity was assessed by histochemical assay to evaluate senescence in undifferentiated and differentiated GFP$^+$PDGFRα$^+$ co-positive cells. The experimental procedure was performed as suggested by the Manufacturer and described in Star Methods. Senescent cells stain a blue color (black arrows). Scale bar 100μm. The graph represents the percentage of senescent cells per field (each dot represents a different field) in n=3 independent experiments in each condition. Data represent mean ± SD and are analyzed by Student's t-test. Data are not significant (ns). **(E)** Quantitative real time PCR of key myofibroblast transcripts for genes involved in ECM remodeling (*Adam12*) and the fibrotic response (*Tgfβ1, collagen1a1 and Fap*) comparing differentiated *vs* undifferentiated PDGFRα$^+$ cells. 2ng/microliter of amplified cDNA was used in each reaction. Samples were normalized against *18sRNA* transcript levels and relative expression was calculated with the 2^{-DDCt} formula. Student's t-test was performed using Prism 6.0. For *Fap* *P=0.035. For *Adam12* **P=0.0013. For *Collagen1a1* **P=0.0085. For *Tgfβ1* *P=0.03. Data represent mean ± SD and are from n=3 independent experiments for both cell types. **(F)** Representative single channel immunofluorescence images are shown and correspond to the merged panels in Figure 6F-H. In brief, we performed adoptive transfer and locally injected differentiated myofibroblast-like GFP$^+$PDGFRα$^+$ cells from *PdgfrαH2B-eGfp* mice into young 3 month old nude mice 24 hours after HLI. Tissues were harvested after 21 days. Adductor muscles were frozen in OCT and 8μm sections were labeled overnight with anti-GFP FITC-conjugated antibody and anti-collagen1 polyclonal antibody. Alternatively, control staining for collagen1 was performed using rabbit IgG as primary antibody at the same concentration as the anti-collagen1 antibody. DAPI was used to stain nuclei. Imaging was acquired with a Leica CTR 5500 microscope and DFC340FX camera. Scale bar 20μm in all pictures. **(G)** Quantification, per field, of mesh area (total tube area), total branching (amount of branches expanding from the nodes) and number of junctions (extent of vessel branching) of HUVECs grown in basal media that were then embedded in Matrigel with no added media (comparator group), or conditioned media from cultured undifferentiated versus differentiated GFP$^+$PDGFRα$^+$ cells. Endpoints were assessed after 7 hours in matrigel. ImageJ angiogenesis software was used for quantification. No statistical differences were observed in mesh area (P=0.17), total branching (P=0.59) and number of junctions (P=0.60). Data represent n=3 independent experiments and were compared by Student's t-test. Data represent mean ± SD. **(H)**

Quantitative real time PCR of pro-angiogenic transcripts *Angiogenin* and *Vegf-A in vivo* in $GFP^{+}PDGFR\alpha^{+}$ cells under physiological (SM) and ischemic (SMI) hindlimb conditions from *PdgfrαH2B-eGfp* mice. Analysis of amplified cDNA was performed using Taqman probes specific for the indicated genes (Thermo Fisher Scientific). Data represent n=4 independent experiments and were compared by Student's t-test. Data are not significant (ns) and represent mean ± SD. For *Angiogenin* P=0.21 and for *Vegf-A* P=0.98.

Figure S7

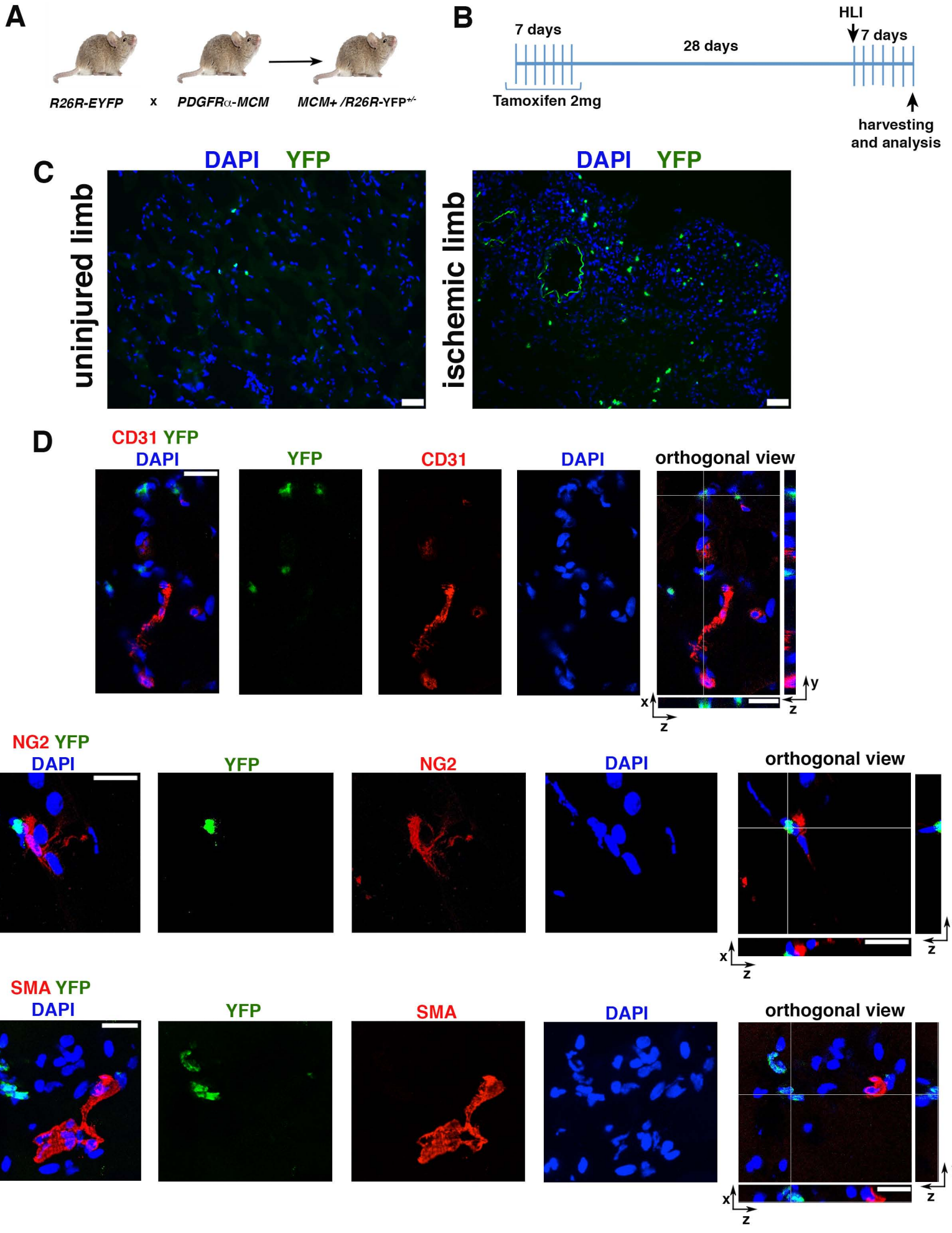
A
R26R-EYFP
x
PDGFRα-MCM
MCM+ /R26R-YFP+/-
B
7 days
28 days
HLI
7 days
Tamoxifen 2mg
harvesting
and analysis
C
DAPI YFP
uninjured limb
DAPI YFP
ischemic limb
D
CD31 YFP
DAPI
YFP
CD31
DAPI
orthogonal view
E
NG2 YFP
DAPI
YFP
NG2
DAPI
orthogonal view
F
SMA YFP
DAPI
YFP
SMA
DAPI
orthogonal view

Figure S7. Lineage tracing of PDGFRα$^+$ cells in physiological conditions in adult skeletal muscle. Related to Figures 7 and S8. **(A)** Breeding strategy to generate *MCM$^+$/R26R-YFP$^{+/-}$* mice harboring a knockin for *CreER* in the *Pdgfrα* locus. **(B)** To induce YFP expression in PDGFRα$^+$ cells, *MCM$^+$/R26R-YFP$^{+/-}$* mice were treated with tamoxifen as indicated. HLI was performed 28 days after the final tamoxifen injection, and sample collection was performed 7 days after HLI. Apart from (C), results following HLI are presented in Figure S8. **(C)** Representative immunofluorescent analysis of *MCM$^+$/R26R-YFP$^{+/-}$* mice in uninjured control limb (left panel) and ischemic limb (HLI, right panel). In uninjured (control) mice there were scattered YFP$^+$ cells present (left panel). Following HLI (right panel) we observed a significant increase in the number of YFP$^+$ cells in the injured area (the green circular structure is auto-fluorescent signal from the elastic lamina of a small artery). Scale bars are 50μm. Images were acquired with a Leica DMi8, Application Suite X and DCM2900 camera. **(D)** Confocal z-stacked images of tamoxifen-induced control *MCM$^+$/R26R-YFP$^{+/-}$* mice without HLI, showing no co-positive staining between YFP and CD31. Corresponding x-y, x-z and y-z orthogonal views represent overlays of the three fluorescent channels (green, blue and red) and were snapshot in specific z-stack layers displaying potential co-staining events. Measurements for the orthogonal views are as follows: 132.5x4.6μm for y-z axes and 74.8x4.6μm for x-z axes. **(E)** Confocal z-stacked images of tamoxifen-induced control *MCM$^+$/R26R-YFP$^{+/-}$* mice without HLI showing no co-positive staining between YFP and NG2, including the corresponding orthogonal views as described above. Measurements for the orthogonal views are: 62.7x7.2μm for y-z axes and 75x7.2μm for x-z axes. **(F)** Confocal z-stacked images of tamoxifen-induced control *MCM$^+$/R26R-YFP$^{+/-}$* mice without HLI showing no co-positive staining between YFP and αSMA, including corresponding orthogonal views. Measurements for the orthogonal views are: 94.8x14.2μm for y-z axes and 110.9x14.2μm for x-z axes. Grid lines across all orthogonal images show the cross-sectional coordinates where YFP$^+$ cells were analyzed for stromal and vessel marker co-expression. Orthogonal views were reconstructed from the acquired z-stacks using Fiji. Images in panels D-F were acquired with Leica SP5 DM confocal microscope, with all sections being of 10μm in thickness and scale bars 20μm. GFP-FITC, CD31, NG2 and αSMA-CY3 antibodies were used as indicated in Star Methods. For Figures S7 and S8, images are representative of analyses performed in 4 independent mice for each condition.

Figure S8

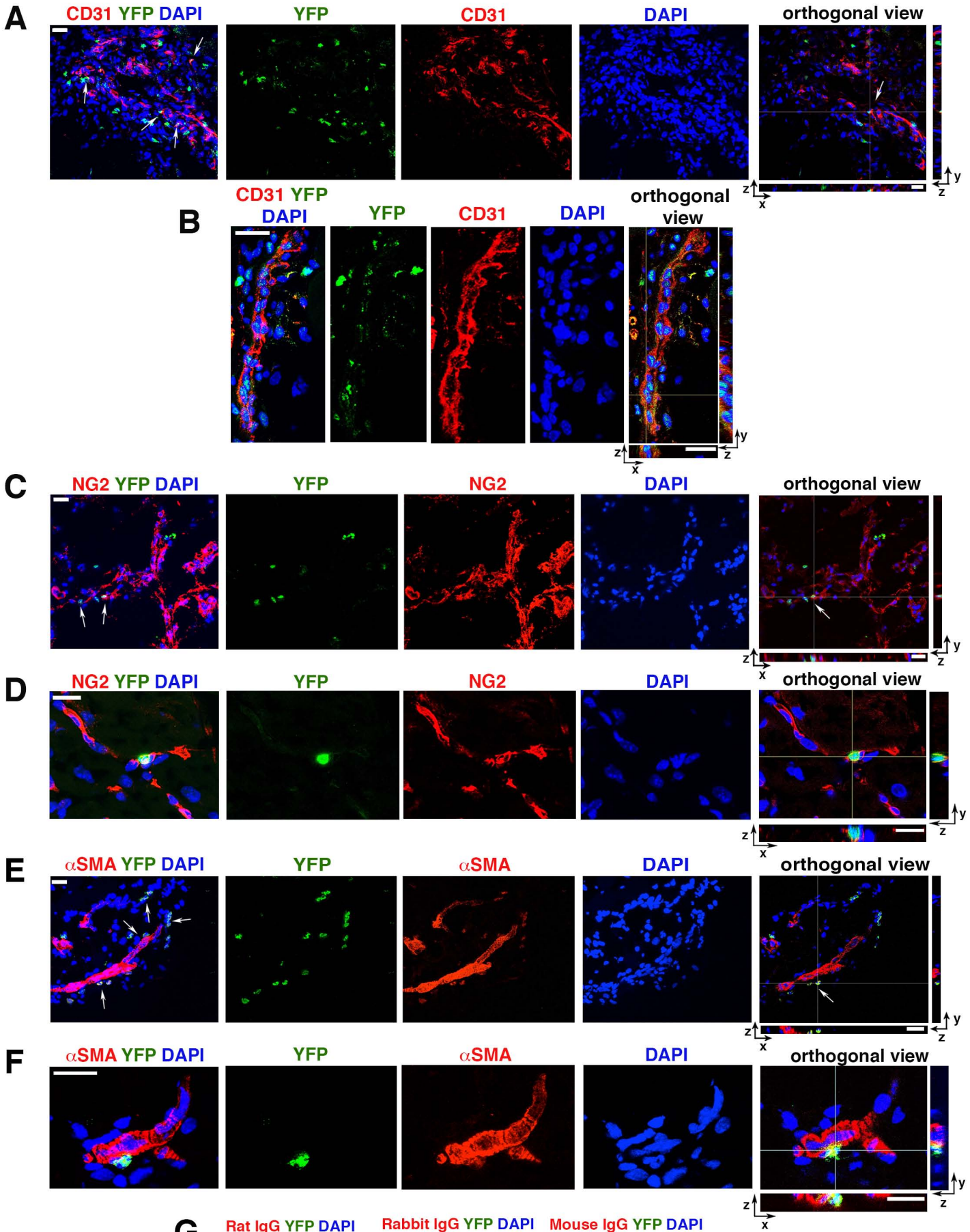
A
CD31 YFP DAPI
YFP
CD31
DAPI
orthogonal view
B
CD31 YFP DAPI
YFP
CD31
DAPI
orthogonal view
C
NG2 YFP DAPI
YFP
NG2
DAPI
orthogonal view
D
NG2 YFP DAPI
YFP
NG2
DAPI
orthogonal view
E
αSMA YFP DAPI
YFP
αSMA
DAPI
orthogonal view
F
αSMA YFP DAPI
YFP
αSMA
DAPI
orthogonal view
G
Rat IgG YFP DAPI
Rabbit IgG YFP DAPI
Mouse IgG YFP DAPI

Figure S8. PDGFRα^{+} cells are present in the stromal and vascular compartments after ischemic insult in adult skeletal muscle. Related to Figures 7 and S7. As shown in Figure S7, *MCM^{+}/R26R-YFP$^{+/-}$* mice harboring a knockin for *CreER* in the *Pdgfrα* locus received tamoxifen and HLI was performed 28 days after final tamoxifen injection. Sample collection was performed 7 days after HLI. Results from uninjured (control) mice are presented in Figure S7. 3D-microscopy images are presented as overlays, single color images, and as x-y, x-z and y-z orthogonal views (as per Figure S7). Orthogonal views were reconstructed from the acquired z-stacks using Fiji. Grid lines across all orthogonal images show the cross-sectional coordinates where YFP^{+} cells were analyzed for stromal and vessel marker co-expression. All sections are 10μm in thickness and all scale bars are 20μm. Confocal images were acquired as z-stacks with a Leica SP5 DM microscope. GFP-FITC, CD31, NG2 and αSMA-CY3 antibodies were used as indicated in Star Methods. For low power views, arrows are used to indicate co-positive cells. **(A)** low and **(B)** high power views showing YFP and CD31 co-expression after HLI. Measurements for orthogonal views are: 246.3x8.4μm for y-z and 246.3x8.4μm for x-z axes (low power view), and 169.3x8.4μm for y-z and 66.4x8.4μm for x-z axes (high power view). **(C)** low and **(D)** high power views showing YFP and NG2 co-expression after HLI. Measurements for orthogonal views are: 246.3x8.9μm for y-z and 246.3x8.9μm for x-z axes (low power view), and 81.77x10.3μm for y-z and 105.8x10.3μm for x-z axes (high power view). **(E)** low and **(F)** high power views showing YFP and αSMA co-expression after HLI. Measurements for orthogonal views are: 246.3x10.1μm for y-z and 246.3x10.1μm for x-z axes (low power view), and 57.7x8.9μm for y-z and 72.8x8.9μm for x-z axes (high power view). **(G)** Z-stack images of control immunoglobulins for CD31 (Rat IgG), NG2 (Rabbit IgG) and αSMA (Mouse IgG). Staining was performed with IgG control antibodies as described in Star Methods.

Figure S9

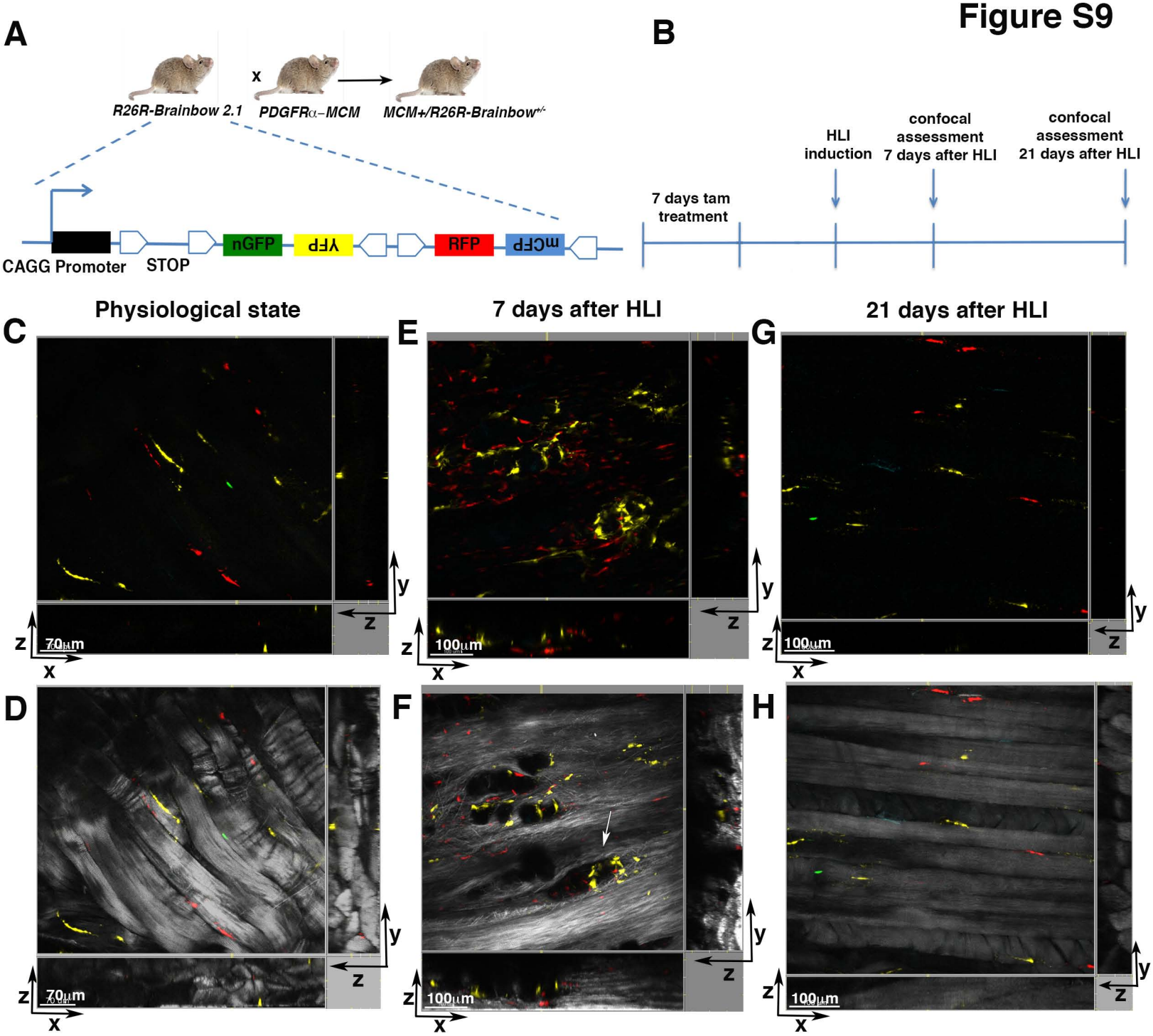
A
R26R-Brainbow 2.1
x
PDGFRα–MCM
MCM+/R26R-Brainbow+/-
CAGG Promoter
STOP
nGFP
YFP
RFP
mCFP
B
7 days tam treatment
HLI induction
confocal assessment 7 days after HLI
confocal assessment 21 days after HLI
Physiological state
7 days after HLI
21 days after HLI
C
D
E
F
G
H
70µm
100µm
x
y
z

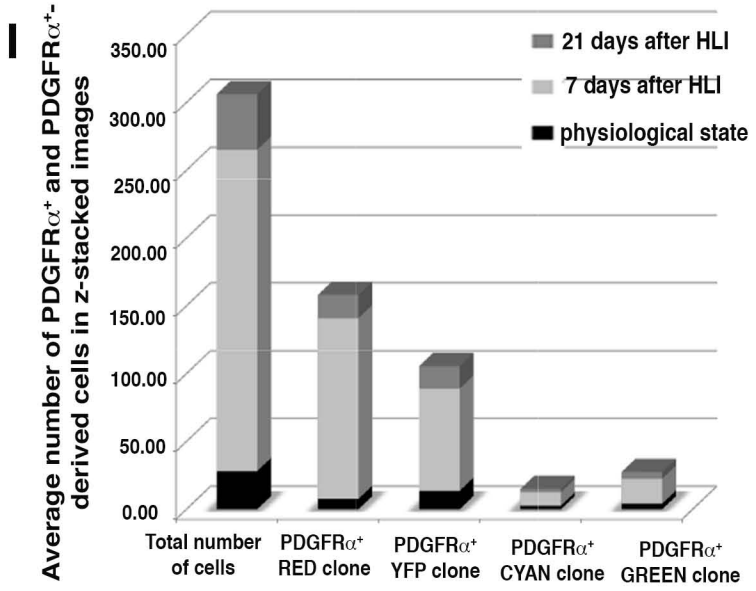
I
Average number of PDGFRα+ and PDGFRα+-derived cells in z-stacked images
350.00
300.00
250.00
200.00
150.00
100.00
50.00
0.00
21 days after HLI
7 days after HLI
physiological state
Total number of cells
PDGFRα+ RED clone
PDGFRα+ YFP clone
PDGFRα+ CYAN clone
PDGFRα+ GREEN clone

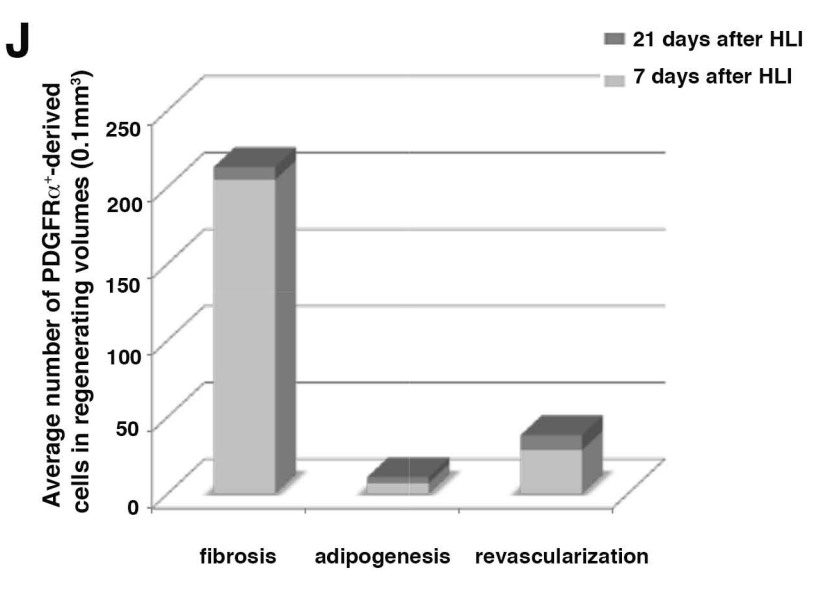
J
Average number of PDGFRα+-derived cells in regenerating volumes (0.1mm3)
250
200
150
100
50
0
21 days after HLI
7 days after HLI
fibrosis
adipogenesis
revascularization

Figure S9. PDGFRα$^+$-derived cells undergo expansion after ischemia-induction. Related to Figure 7. **(A)** Breeding strategy to generate *MCM$^+$/R26R-Brainbow$^{+/-}$* mice where PDGFRα$^+$ cells and their progeny permanently express one of four fluorescent proteins. The Brainbow 2.1 region contains two *loxP*-flanked dimers, positioned head-to-tail in tandem. One dimer has nuclear-localized green fluorescent protein (nGFP) and a reverse-oriented cytoplasmic yellow fluorescent protein (YFP). The other dimer has cytoplasmic red fluorescent protein (RFP) and a reverse-oriented membrane-cyan fluorescent protein (mCFP). **(B)** Tamoxifen treatment to activate PDGFRα-Cre-mediated recombination of the Brainbow cassette. Tam, tamoxifen. Tamoxifen was administered for 7 consecutive days and HLI was induced 4-5 days after last injection of tamoxifen. Two-photon confocal microscopy was performed on uninjured hindlimbs (physiological state) and at 7 and 21 days after HLI. **(C-H)** 3D-microscopy images are presented as x-y, x-z and y-z views. Paired images of the overlayed four fluorescent channels alone (C, E, G; pseudocolored in cyan for CFP, green for GFP, yellow for YFP, red for RFP) and the corresponding merged-second harmonic generation (SHG, white) images (D, F, H) are displayed. All four fluorescent Brainbow recombined PDGFRα$^+$ clones were observed in physiological (uninjured) conditions (C, D) aligned along skeletal muscle fibers. 7 days after HLI, expansion of PDGFRα$^+$ cells occurred in the CFP$^+$, GFP$^+$, YFP$^+$ and RFP$^+$ clones (E, F, I), that were found to be distributed between the ischemic skeletal muscle fibers and vessels (F). PDGFRα$^+$ cells showed cell-cell and cell-matrix interactions and were associated with vessel-like structures (F, white arrow). 21 days after HLI (G, H), PDGFRα$^+$ cells re-established their original (physiological uninjured) environmental niche in most of the regenerated muscle (H). Images are representative of analyses performed in different locations in 3 independent mice in each condition (physiological state, and, 7 and 21 days after HLI induction) as described in Star Methods. Scale bars as indicated. **(I)** Quantification of the average number of PDGFRα$^+$ and PDGFRα$^+$-derived cells in uninjured tissue and during regeneration after HLI (7 and 21 days). Each cell expressing a single fluorescent protein was automatically segmented as a surface object using Imaris software as described in Star Methods. Lineage-tracked cells were counted in 3 z-stack images for each mouse in different areas of the skeletal muscle for the different conditions (uninjured, 7 and 21 days after HLI, n=3 for each of these conditions). **(J)** The average number of PDGFRα$^+$-derived cells present in injured and regenerating areas was quantified in n=3 independent mice at each time point after HLI (7 and 21 days) using SHG images to distinguish fibrotic, adipocytic and revascularized areas. Quantification was performed by counting PDGFRα$^+$-derived fluorescent cells present in z-stacked images per 0.1mm^3 volume as described in Star Methods.

Figure S10

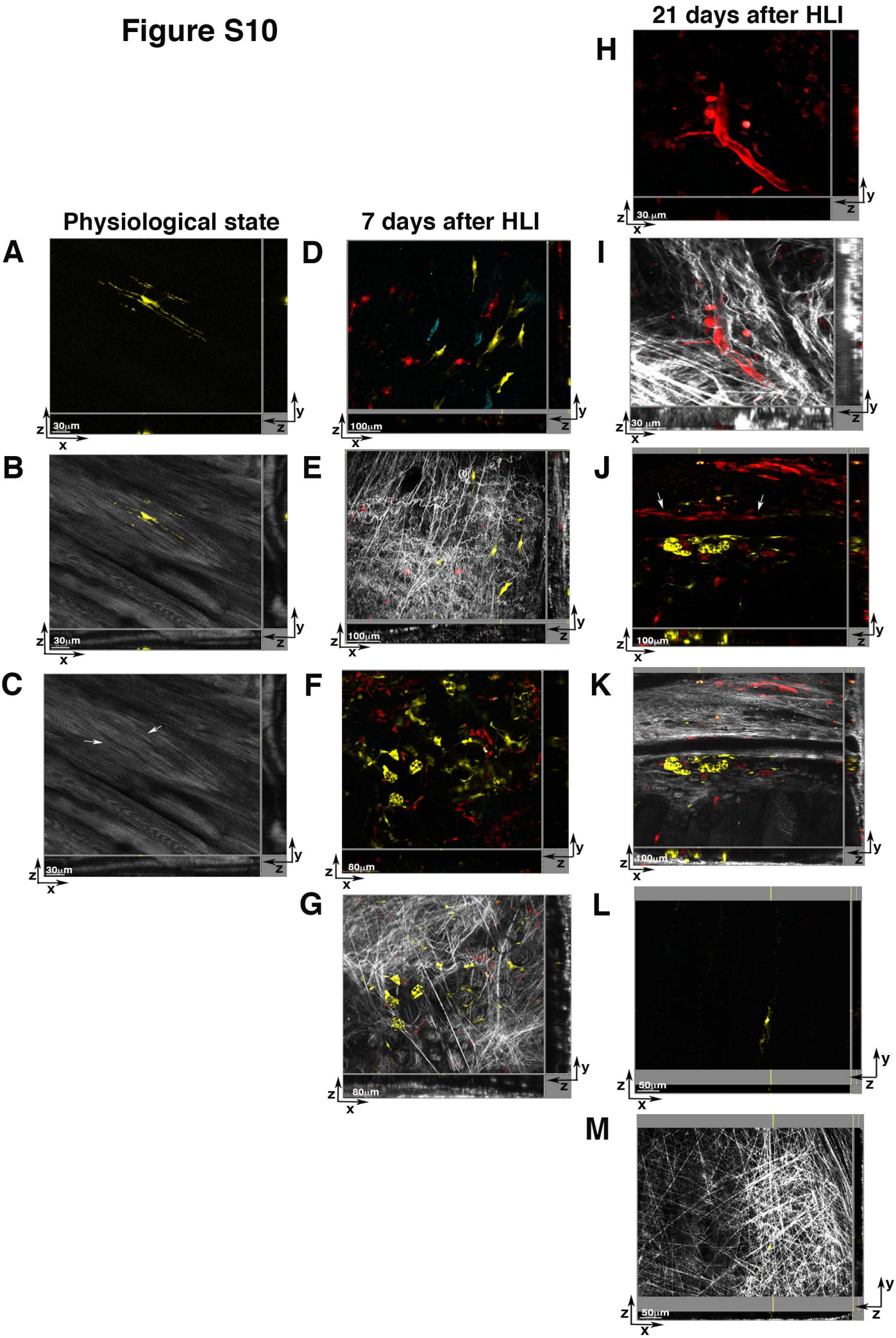
Physiological state
7 days after HLI
21 days after HLI
A
B
C
D
E
F
G
H
I
J
K
L
M
30μm
100μm
80μm
50μm
x
y
z

Figure S10. PDGFRα^{+} cells differentiate into different stromal lineages. Related to Figure 7.
(A-C) Using *MCM^{+}/R26R-Brainbow$^{+/-}$* mice, we observed that in the physiological (uninjured) state PDGFRα^{+} cells were aligned along small capillaries running between skeletal muscle fibers. (A) and (C) represent the fluorescent and SHG x-y-z images, respectively, while (B) is an overlay of these. **(D-E)** Fluorescent (D) and SHG/fluorescent overlay (E) of PDGFRα^{+}-derived cells in a fibrotic area 7 days after HLI. Images show the contribution of RFP^{+}, YFP^{+} and CFP^{+} cells to the fibrotic volume. **(F-G)** Fluorescent (F) and SHG/fluorescent overlay (G) x-y-z images of PDGFRα^{+}-derived cells showing contribution to brown adipose tissue 7 days after HLI. **(H-I)** Fluorescent (H) and SHG/fluorescent overlay (I) x-y-z images of PDGFRα^{+}-derived cells showing their contribution to new vessel formation in areas of tissue remodeling 21 days after HLI. **(J-K)** Fluorescent (J) and SHG/fluorescent overlay (K) x-y-z images of PDGFRα^{+}-derived cells showing contribution to vessels (arrows) and adipose tissue in an area of tissue remodeling 21 days after HLI induction. **(L-M)** Fluorescent (L) and SHG/fluorescent overlay (M) x-y-z images of PDGFRα^{+}-derived cells showing a marked reduction in their contribution to remaining fibrotic areas at 21 days after HLI. All images were analyzed with Imaris x64 software version 8.4 and are representative of analyses performed in different locations in n=3 independent mice in each condition (physiological state, and, 7 and 21 days after HLI induction) as described in Star Methods. Scale bars as indicated.

Table S2. Related to Figure 5 and Figure S5. Analysis of Table S1 gene list (differentially expressed genes from $GFP^{+}PDGFR\alpha^{+}$ co-positive cells isolated from uninjured hindlimbs versus 7 days after HLI) according to the Molecular Signature data base (mSigDB) showing all significantly activated signatures.

Class	Gene Set	Gene Set Size	Expected Hits	Observed Hits	OR	Pvalue
mSigDB c2	NABA_MATRISOME	587	12.81973476	57	4.44626984	6.18E-22
mSigDB c2	BOQUEST_STEM_CELL_CULTURED_VS_FRESH_UP	352	7.687472971	44	5.72359736	2.75E-21
Mouse_Gene_Atlas	osteoblast_day21	219	4.782831195	28	5.854273099	4.02E-14
mSigDB c2	NABA_CORE_MATRISOME	195	4.258685311	26	6.105170517	1.25E-13
mSigDB c2	LEE_BMP2_TARGETS_UP	636	13.88986594	46	3.311767026	5.99E-13
mSigDB c2	WONG_ADULT_TISSUE_STEM_MODULE	601	13.12548652	44	3.35225669	1.34E-12
Mouse_Gene_Atlas	osteoblast_day14	239	5.219619432	27	5.172790919	2.37E-12
mSigDB c2	LIM_MAMMARY_STEM_CELL_UP	403	8.801282975	34	3.863073156	1.32E-11
mSigDB c2	BOQUEST_STEM_CELL_UP	230	5.023064725	25	4.977041182	3.73E-11
mSigDB c2	CHIARADONNA_NEOPLASTIC_TRANSFORMATION_CDC25_UP	113	2.467853539	18	7.293787786	4.01E-11
Mouse_Gene_Atlas	umbilical_cord	114	2.489692951	18	7.229807191	4.67E-11
mSigDB c2	SARRIO_EPITHELIAL_MESENCHYMAL_TRANSITION_DN	116	2.533371775	18	7.105155343	6.30E-11
mSigDB c2	NABA_ECM_GLYCOPROTEINS	139	3.035678247	19	6.258897832	1.77E-10
GO_Cellular_Component_2013	extracellular region part (GO:0044421)	248	5.416174139	25	4.615804322	1.91E-10
mSigDB c2	CHEN_LVAD_SUPPORT_OF_FAILING_HEART_UP	81	1.76899236	15	8.479403496	1.93E-10
mSigDB c2	NABA_MATRISOME_ASSOCIATED	392	8.561049445	31	3.621051391	5.61E-10
mSigDB c2	OSWALD_HEMATOPOIETIC_STEM_CELL_IN_COLLAGEN_GEL_UP	193	4.215006487	21	4.982198738	1.42E-09
mSigDB c2	ONDER_CDH1_TARGETS_2_UP	224	4.892028254	22	4.497112211	3.98E-09
mSigDB c2	CHICAS_RB1_TARGETS_CONFLUENT	479	10.46107828	33	3.154550528	5.06E-09
mSigDB c2	SCHUETZ_BREAST_CANCER_DUCTAL_INVASIVE_UP	298	6.508144731	25	3.84134051	8.73E-09
mSigDB c2	SWEET_LUNG_CANCER_KRAS_DN	353	7.709312383	27	3.502257875	1.57E-08
mSigDB c2	GERY_CEBP_TARGETS	113	2.467853539	15	6.078156488	2.29E-08
mSigDB c2	SEKI_INFLAMMATORY_RESPONSE_LPS_UP	69	1.506919418	12	7.963265892	2.75E-08
mSigDB c2	GAJATE_RESPONSE_TO_TRABECTEDIN_UP	56	1.223007064	11	8.994224422	2.79E-08
mSigDB c2	SMID_BREAST_CANCER_LUMINAL_B_DN	354	7.731151795	26	3.363017658	6.65E-08
mSigDB c2	TURASHVILI_BREAST_LOBULAR_CARCINOMA_VS_DUCTAL_NORMAL_UP	61	1.332204123	11	8.256992912	7.12E-08
mSigDB c2	ANASTASSIOU_CANCER_MESENCHYMAL_TRANSITION_SIGNATURE	61	1.332204123	11	8.256992912	7.12E-08
mSigDB c2	HAN_SATB1_TARGETS_UP	313	6.835735909	24	3.510960681	9.75E-08
mSigDB c2	WESTON_VEGFA_TARGETS	80	1.747152948	12	6.868316832	1.51E-07
mSigDB c2	SERVITJA_ISLET_HNF1A_TARGETS_UP	130	2.83912354	15	5.28332064	1.53E-07
Reactome_2015	Extracellular matrix organization	213	4.651794724	19	4.084445064	2.17E-07
mSigDB c2	GAUSSMANN_MLL_AF4_FUSION_TARGETS_E_UP	84	1.834510595	12	6.541254125	2.63E-07
mSigDB c2	LINDVALL_IMMORTALIZED_BY_TERT_DN	69	1.506919418	11	7.299660401	2.66E-07
mSigDB c2	NUYTTEN_EZH2_TARGETS_UP	859	18.76005478	43	2.292104181	2.76E-07
mSigDB c5	EXTRACELLULAR_REGION_PART	197	4.302364134	18	4.183746293	3.19E-07
mSigDB c2	TONKS_TARGETS_OF_RUNX1_RUNX1T1_FUSION_HSC_UP	160	3.494305896	16	4.578877888	4.31E-07
mSigDB c2	PLASARI_TGFB1_TARGETS_10HR_UP	183	3.996612368	17	4.253602409	5.39E-07
mSigDB c2	CROMER_TUMORIGENESIS_UP	46	1.004612945	9	8.958674128	5.44E-07
mSigDB c2	ZHU_CMV_24_HR_DN	75	1.637955889	11	6.715687569	6.36E-07

mSigDB c3	AACTTT_UNKNOWN	1409	30.7717313	59	1.917344183	6.38E-07
mSigDB c2	BROWNE_HCMV_INFECTION_24HR_DN	126	2.751765893	14	5.087642098	6.38E-07
mSigDB c7	GSE8515_IL1_VS_IL6_4H_STIM_)MAC_UP	166	3.625342367	16	4.413376277	7.11E-07
mSigDB c2	SANA_TNF_SIGNALING_UP	61	1.332204123	10	7.506357193	7.16E-07
mSigDB c2	STEGER_ADIPOGENESIS_DN	25	0.545985296	7	12.82085809	7.58E-07
mSigDB c2	LI_WILMS_TUMOR_VS_FETAL_KIDNEY_2_DN	48	1.048291769	9	8.58539604	7.97E-07
mSigDB c5	EXTRACELLULAR_REGION	255	5.569050022	20	3.591276775	8.24E-07
mSigDB c7	GSE360_HIGH_DOSE_B_MALAYI_VS_M_TUBERCULOSIS_MAC_DN	149	3.254072366	15	4.609608612	9.13E-07
mSigDB c2	WANG_SMARCE1_TARGETS_UP	234	5.110422373	19	3.717892302	9.25E-07
mSigDB c2	VECCHI_GASTRIC_CANCER_ADVANCED_VS_EARLY_UP	150	3.275911777	15	4.578877888	9.94E-07

Table S3. Related to Figure 7 and Figure S9. Percentages of individual fluorescent cells in physiological conditions and 7 and 21 days after HLI quantified as described in Star Methods.

	%RFP	%YFP	%CFP	%GFP
Physiological	27.20	48.52	9.47	14.80
7 days after HLI	56.24	31.78	4.22	7.73
21 days after HLI	41.8	40.4	5.58	12.19